

Altermagnetism: a third magnetic class delimited by spin symmetry groups

Libor Šmejkal,^{1,2} Jairo Sinova,^{1,2} and Tomas Jungwirth^{2,3}

¹*Institut für Physik, Johannes Gutenberg Universität Mainz, 55128 Mainz, Germany*

²*Institute of Physics, Czech Academy of Sciences,
Cukrovarnická 10, 162 00, Praha 6, Czech Republic*

³*School of Physics and Astronomy, University of Nottingham,
NG7 2RD, Nottingham, United Kingdom*

(Dated: May 13, 2021)

Modern research areas, ranging from topological condensed matter and dissipationless quantum transport to spintronics, are built on a magnetic symmetry group theory which entangles magnetism and relativistic spin-orbit coupling. Here we return to the non-relativistic foundations of collinear magnetism and delimit Type-I spin groups containing no spin-rotation symmetry element, Type-II with a spin-rotation symmetry, and Type-III with symmetry elements combining spin and crystal rotations. We show that they describe, respectively, ferromagnets with spin-polarized electron bands, antiferromagnets with spin-degenerate bands, and a third class with alternating spin-polarizations in locked momentum and crystal space. We refer to the third class as altermagnets and identify their topological invariants which have a form of an even-integer spin winding number in the momentum space. Our band structure analysis reveals a spin splitting by an electrostatic crystal field as a unique spectroscopy signature of altermagnetism. We find altermagnetic material candidates ranging from high Néel temperature insulators and metals to a parent cuprate of high-temperature superconductivity.

In the 1930s, Néel introduced to magnetism a notion of a local molecular field, whose sign can flip from one magnetic sublattice to another [1]. His work was prompted by earlier observations of anomalous responses in some magnetic crystals and was based on Heisenberg's non-relativistic theory of short-range exchange interaction [1]. Néel's phenomenology combined with formal symmetry arguments led to the delimitation within the family of magnetic crystals of the class known as antiferromagnets, as described, e.g., in Ref. [2]. Taking an example of two antiparallel magnetic sublattices, antiferromagnets are crystals in which atoms in these two sublattices are connected by a crystal symmetry operation; otherwise, symmetry would not require the Heisenberg exchange to generate strictly equal magnitudes of the sublattice magnetic moments, and the crystal would be ferromagnetic [2]. To date, this has remained the fundamental boundary line in non-relativistic magnetism, separating the two basic classes of ferromagnets and antiferromagnets.

Relativistic effects typically complement the exchange-driven magnetism in a perturbative manner. Here a prominent example is the magnetocrystalline anisotropy contribution to the total energy which defines the preferred crystallographic direction of the magnetic order vector [2]. Modern research focuses on more exotic strongly relativistic phenomena, such as Weyl fermion quasiparticles and momentum-space magnetic monopoles, or magnetic topological insulators and the quantum anomalous Hall effect [3–5]. Relativistic magnetic symmetry groups, considering coupled real-space and spin-space symmetry operations, have become the broadly applied basic theory tool in the field [6–9].

In this paper we return to the fundamentals of non-relativistic magnetism and draw a second boundary line, complementing the traditional division into ferromagnetic and antiferromagnetic classes. Since in the magnetic group theory, ferromagnetism, antiferromagnetism and relativistic effects are entangled, we take a different theory approach based on a non-relativistic spin group formalism [6, 10, 11]. In contrast to the magnetic groups, we construct spin groups for collinear magnets by a decomposition into non-transposing symmetries, which transform a

magnetic sublattice on itself, and inter-sublattice transposing symmetries. Our spin groups are designed to classify the momentum and spin-dependent band structure of the magnets. We obtain Type-I groups describing ferromagnets with spin-polarized electron bands, Type-II groups corresponding to antiferromagnets with spin-degenerate bands, and Type-III groups delimiting a third magnetic class with alternating spin-polarizations in locked momentum and crystal space. We refer to the third class as altermagnets and identify distinct topological invariants of their spin-momentum interaction.

We also highlight their unique spectroscopy signature in the form of momentum-dependent spin splitting by an electrostatic crystal field. Our spin group decomposition into the non-transposing and transposing symmetries is ideally suited to guide us towards materials with the presence and large strength of this prominent spectroscopy signature. The non-transposing symmetries define local sublattice crystalline anisotropies and, together with the transposing symmetries, govern the optimal mutual tilt between the sublattice anisotropies and the type of chemical orbitals that maximize the spin-polarization in the momentum space of altermagnets.

To illustrate the broad materials landscape of altermagnetism, and its potential interplay with other macroscopic quantum phases, we present symmetry, topology, and spectroscopy analysis, and *ab initio* calculations in candidate materials ranging from a quasi-one-dimensional ruthenate KRu_4O_8 and insulating distorted rutile CuF_2 , to a high Néel temperature bi-metallic CrSb and a parent cuprate of high-temperature superconductivity La_2CuO_4 with quasi-two-dimensional crystal planes.

We note that several recent works reported anomalous characteristics and responses in some collinear antiferromagnets. These intriguing observations include Hall effect [12–15] and spin splitting in the *ab initio* non-relativistic band structure [12, 14–23], as well as predictions of conserved spin-currents and giant magnetoresistance in the absence of a net equilibrium magnetization [24–28]. Our general symmetry, topology, and spectroscopy theory establishes that, rather than exotic antiferromagnetic anomalies in some materials, the reports exemplify the

phenomenology of the separate class of altermagnets, formally delimited in our work.

Altermagnetic spin groups and topology. We construct the non-relativistic spin point groups from the crystallographic symmetry groups by adding a rotation symmetry operation in the spin space, which is decoupled from the real space. For the important family of collinear magnets [2], on which we focus in this paper, the only operation in the spin space we need to consider is a 180° spin rotation \mathcal{R}_s . We further consider the centrosymmetric spin point groups, i.e., the ones that have always \mathcal{P} among the elements. These are relevant for the collinear magnets with the \mathcal{TR}_s -symmetry, where \mathcal{T} is time-reversal [21, 29, 30]. For the momentum (wavevector \mathbf{k}) and spin (\mathbf{s}), the \mathcal{TR}_s -symmetry acts as the \mathcal{P} -symmetry, where \mathcal{P} is space inversion: $E(\mathbf{k}, \mathbf{s}) = \mathcal{TR}_s E(\mathbf{k}, \mathbf{s}) = \mathcal{P} E(\mathbf{k}, \mathbf{s})$.

We obtain three types of centrosymmetric spin point groups, classifying the momentum and spin-dependent band structure of collinear non-relativistic magnets. They differ by the kind of symmetry operations they contain. These are either non-transposing crystal symmetry elements, \mathcal{A}_e , which transform a magnetic sublattice on itself (or on a sublattice with the same magnetic moment orientation). The other elements transpose sublattices with opposite magnetic moment orientations, and are labelled \mathcal{A}_o . The transposing elements are crystal symmetry operations that guarantee the equal magnitude of the magnetic moments on the sublattices transposed by \mathcal{A}_o [2]. The transposing symmetry operations \mathcal{A}_o appear in combination with \mathcal{R}_s which imposes the opposite sign of the magnetic moments on the two sublattices. The three types of the centrosymmetric spin point groups have a distinct structure with respect to \mathcal{R}_s :

We define Type-I centrosymmetric spin point groups as, $S_I = G$, where G is a centrosymmetric crystallographic point group. Type-I groups do not have the \mathcal{R}_s -symmetry, alone or in any combination with a crystal symmetry operation. There is no transposing symmetry in Type-I groups. Consequently, the non-transposing \mathcal{A}_e -symmetries in S_I do not enforce spin-degeneracy in the momentum space, because they do not connect energy eigenstates with the same momentum and opposite spin. Therefore, the Type-I centrosymmetric spin point groups

correspond to collinear non-relativistic ferromagnets with spin-polarized bands, as illustrated in Fig. 1. There are 11 Type-I centrosymmetric spin point groups.

Type-II centrosymmetric spin point groups are defined as, $S_{\text{II}} = G \oplus G\mathcal{R}_s$, i.e., there is also 11 Type-II groups. They have the \mathcal{R}_s -symmetry and correspond to non-magnetic non-relativistic crystals with spin-unpolarized bands over the entire Brillouin zone, since $E(\mathbf{k}, \mathbf{s}) = \mathcal{R}_s E(\mathbf{k}, \mathbf{s}) = E(\mathbf{k}, -\mathbf{s})$. In addition, we find that they also describe antiferromagnets, as illustrated in Figs. 1, with spin-unpolarized bands due to the $t\mathcal{R}_s$ or $\mathcal{P}\mathcal{R}_s$ symmetry. In the former case, t is a translation which transposes the sublattices with opposite magnetic moment orientations. The $t\mathcal{R}_s$ -symmetry corresponds to the \mathcal{R}_s -symmetry in the spin point groups. In the latter case, \mathcal{P} is the transposing symmetry. To see that $\mathcal{P}\mathcal{R}_s$ acts as \mathcal{R}_s on the wavevector and spin we recall the \mathcal{P} -invariance and write, $E(\mathbf{k}, \mathbf{s}) = \mathcal{P}\mathcal{R}_s E(\mathbf{k}, \mathbf{s}) = E(-\mathbf{k}, -\mathbf{s}) = \mathcal{P}E(-\mathbf{k}, -\mathbf{s}) = E(\mathbf{k}, -\mathbf{s}) = \mathcal{R}_s E(\mathbf{k}, \mathbf{s})$. In other words, the spin point group with \mathcal{P} and $\mathcal{P}\mathcal{R}_s$ elements has to contain also the $\mathcal{P}^2\mathcal{R}_s = \mathcal{R}_s$ symmetry element, since $\mathcal{P}^2 = \mathcal{E}$ (\mathcal{E} is identity).

Finally, we arrive at Type-III centrosymmetric spin point groups which we define as,

$$S_{\text{III}} = H \oplus (G - H)\mathcal{R}_s = H \oplus H\mathcal{A}_o\mathcal{R}_s. \quad (1)$$

Here H is a halving subgroup of G containing non-transposing crystal symmetry elements \mathcal{A}_e . $G - H$ contains transposing elements \mathcal{A}_o , which are crystal rotations (proper or improper). The second equality in Eq. (1) follows from the sublattice decomposition [31] of S_{III} . As illustrated in Figs. 1, the Type III centrosymmetric spin point groups correspond to the collinear non-relativistic altermagnets with alternating spin-polarizations in real and momentum spaces locked by the spin symmetries. The spin-polarization is allowed for momenta satisfying $\mathcal{A}_o\mathbf{k} \neq \mathbf{k}$, i.e., for momenta whose little symmetry group does not contain \mathcal{A}_o . (The little spin point group at a given momentum is a sub-group of the spin point group with operations that transform the momentum on itself or a momentum separated by a reciprocal lattice vector.)

The list of the 10 Type-III centrosymmetric spin point groups describing altermagnets is given in Tab. 1. Note that we adapted the notation from the magnetic point groups [6] to our

spin point groups. Instead of the primed symbols in magnetic groups corresponding to elements with the crystal symmetry operation combined with \mathcal{T} , we have a superscript s corresponding to crystal operations combined with \mathcal{R}_s . Since we are employing only a single symmetry operation in the spin space (\mathcal{R}_s), our centrosymmetric spin point groups have formally the same structure as the centrosymmetric magnetic point groups [6]. However, we emphasize that the rotations are applied jointly in the real and spin spaces in the relativistic magnetic groups, while \mathcal{R}_s is the only operation acting in the spin space in our non-relativistic spin groups.

The altermagnetic spin point groups allow us to determine the spin-momentum interaction locally near the Γ -point, plus additional prominent features such as spin-unpolarized nodal surfaces/lines across the entire Brillouin zone. The Γ -point itself is invariant under all crystal symmetry operations. The $\mathcal{A}_o\mathcal{R}_s$ symmetry present in any altermagnetic spin point group thus guarantees spin-degeneracy of the Γ -point. On the other hand, as pointed out above, spin-polarization in the rest of the Brillouin zone, including other \mathcal{T} -invariant momenta, is not generally excluded in altermagnets. We have also already derived above that the bands are inversion symmetric. Moreover, the collinearity implies that in the non-relativistic altermagnets, spins have a common \mathbf{k} -independent quantization axis. These basic spin-momentum interaction characteristics are in striking contrast to the non-magnetic relativistic crystals with inversion-asymmetry, whose all \mathcal{T} -invariant momenta are spin-degenerate, and the spin-momentum interaction is odd in \mathbf{k} and has a form of a continuously varying spin-polarization texture [32].

We note that the qualitative distinction from the relativistic spin-momentum interaction can facilitate a direct identification of altermagnetism by spin and angle-resolved photoemission spectroscopy measurements. The experimental feasibility is further supported below in the section discussing material candidates, where we complement the symmetry analysis by the demonstration of large spin-splitting magnitudes in altermagnets. They can exceed the strongest bulk spin splittings due to the relativistic spin-orbit coupling by an order of magnitude [33].

The distinct topology of the spin-momentum interaction in altermagnets is determined by

the $\mathcal{A}_o\mathcal{R}_s$ transposing symmetries present in the given spin point group. For example, a mirror transposing symmetry $\mathcal{M}_c\mathcal{R}_s$, where c is the axis perpendicular to the $a-b$ mirror plane, defines a spin-unpolarized $k_a - k_b$ nodal plane at $k_c = 0$, or other k_c separated from $\mathcal{M}_c k_c = -k_c$ by a reciprocal lattice vector. This is because a wavevector from this plane is transformed by $\mathcal{M}_c\mathcal{R}_s$ on itself, or on an equivalent momentum separated by the reciprocal lattice vector, while spin is reversed. Similarly, a $\mathcal{C}_{n,c}\mathcal{R}_s$ symmetry, where $\mathcal{C}_{n,c}$ is an n -fold rotation symmetry around the c -axis, imposes a spin-unpolarized nodal-line parallel to the k_c -axis for wavevectors with $k_a = k_b = 0$, or other $k_{a(b)}$ separated from $\mathcal{C}_{n,c}k_{a(b)}$ by a reciprocal lattice vector. We note that the high symmetry planes or lines are typically of main focus when assessing the evaluated electronic structure, which may explain why altermagnetism remained unnoticed during the many decades of research of the band theory of solids.

Each of the 10 altermagnetic spin point groups can be assigned one of the topological invariants of the spin-momentum interaction near the Γ -point. In Tab. 1 we show orbital-harmonic representations of the spin-momentum interaction, depicted on top of model energy bands. We obtain either planar-like (cf. relativistic Rashba or Dresselhaus spin-texture) or bulk-like (cf. relativistic Weyl spin-texture) spin-momentum interactions, with a spin winding number $W = 2, 4, \text{ or } 6$, when integrated over a surface near and enclosing the Γ -point. The orbital-harmonic representations also allow us to identify a d -wave, g -wave, or i -wave form of the anisotropic spin-momentum interaction. This highlights that altermagnets can host Fermi liquid instabilities in the anisotropic spin-channel [15, 18, 34]. In Tab. 1 we list the characteristic (not exclusive) anisotropic crystal harmonics [21] for each altermagnetic spin point group.

We note that the planar types of the spin-momentum interaction are relevant for (quasi)two-dimensional and three-dimensional crystals, while the bulk types only for three-dimensional crystals. We also remark, that W inferred from the spin point group is the minimal spin winding number when integrating over any Brillouin zone surface enclosing the Γ -point. Further from the Γ -point, additional band-crossings can result in higher even-integer winding numbers.

Altermagnetic spectroscopy and candidate materials. Our band-theory approach, which disentangles non-relativistic phenomena from the full relativistic description by the spin group formalism, is applicable to a range of physical problems. By employing the collinear spin groups, we have demonstrated their strength when delimiting the altermagnetic symmetry type and identifying the topological invariants in the spin-dependent band structure. The approach also directly guides us to favourable material candidates.

Our list of candidate altermagnets is summarized in Tab. 1. We start with the symmetry/topology analysis and *ab initio* band structure calculations of KRu_4O_8 , which allow us to give a representative demonstration of altermagnetism and its spectroscopy with the characteristic spin splitting by the crystal field. We obtained the electronic structure using a density-functional-theory (DFT) full-potential linearised augmented plane-wave code ELK within local-spin-density approximation [35].

In Fig. 2A we show the real-space crystal structure of KRu_4O_8 as reported in earlier studies [36, 37]. The symmetry of the lattice is body-centred tetragonal (crystal space group $I4/m$). The sublattice anisotropies are related by a mutual planar rotation by the maximum possible angle of 90° . The spin point group of the altermagnetic structure, shown in Fig. 2A, is $4^s/m$. According to Eq. (1), it can be decomposed as,

$$4^s/m = 2/m \oplus 2/m\mathcal{C}_{4z}\mathcal{R}_s. \quad (2)$$

The rotation transposing symmetry $\mathcal{C}_{4z}\mathcal{R}_s$ is highlighted in Fig. 2A. It imposes spin-unpolarized nodal lines parallel to the k_z -axis for $k_x = k_y = 0$, $k_x = k_y = 1/2$, and $k_x = -k_y = 1/2$ (here the wavevectors are in units of π divided by the lattice constant). The latter two correspond to equivalent \mathcal{T} -invariant momenta M_1 and M_2 for $k_z = 0$. On the other hand, the \mathcal{T} -invariant momenta X and Y , corresponding to the directions of the sublattice crystal-anisotropy axes, are highly spin-polarized. Consistently, the little spin point group at the X and Y wavevectors is $2/m$, i.e., does not contain any transposing symmetry element. The resulting topology of the spin-momentum interaction in KRu_4O_8 has a winding number $W = 2$.

The spin-momentum interaction is planar, reflecting the real-space planar mutual rotations of the sublattice anisotropies. In Fig. 2B we confirm these symmetry and topology characteristics by plotting the calculated spin-momentum interaction on top of the *ab initio* Fermi surface in KRu_4O_8 .

In Figs. 2C-F we illustrate on KRu_4O_8 the signature feature of the non-relativistic spectroscopy of altermagnets. We start in Figs. 2C, D from the sublattice and spin projected *ab initio* band structure of the non-magnetic phase. It is consistent with the earlier report in Ref. [37] which showed the presence of Ru t_{2g} orbitals near the Fermi level. The t_{2g} d_{xz} and d_{yz} orbitals are degenerate at the Γ -point which is consistent with the octahedral environment with the tetragonal symmetry [38]. Including spin, the Γ -point is four-fold degenerate in the non-magnetic state. The orbitals split by the crystal field when moving from the Γ -point towards the \mathbf{X} or \mathbf{Y} points. Moreover, because of the mutual planar rotation of the sublattice anisotropies by 90° , momentum \mathbf{X} for a given energy is locked to one sublattice, while the \mathbf{Y} momentum for the same energy is locked to the opposite sublattice, as confirmed in Fig. 2C.

The sublattice and spin-resolved band structures in the altermagnetic phase are plotted in Figs. 2E and 2F, respectively. They highlight the sublattice-spin-momentum locking characteristics of altermagnetic KRu_4O_8 , consistent with the sublattice decomposition in Eq. (2). Fig. 2E shows that the locking of the \mathbf{X} and \mathbf{Y} momenta to opposite sublattices, and the strength of the crystal-field splitting persists in the altermagnetic phase. This is consistent with the little point group $2/m$ of the \mathbf{X} and \mathbf{Y} wavevectors which coincides with the crystal point subgroup of non-transposing symmetries (see Eq. (2)), i.e, the sublattice subgroup H .

In addition, the transition to the altermagnetic phase splits the bands by the local molecular exchange field, and the amplitude of the band-splitting is only weakly momentum-dependent (cf. Figs. 2C, E). By comparing Fig. 2E to Fig. 2F with the spin-projected bands, we observe that a momentum locked to one sublattice is also locked to one spin orientation, as expected from the local nature of the molecular exchange field. Since the strength of the local molecular

exchange field is larger than the crystal-field strength in the studied KRu_4O_8 altermagnet, the spin separation at the \mathbf{X} (\mathbf{Y}) wavevector is not limited by the spin-exchange field but rather by the electrostatic crystal field. We observe a spin separation reaching a 300 meV scale. As highlighted above, this large magnitude is due to the presence near the Fermi level of the anisotropic local orbitals at the two sublattices with the 90° mutual tilt of the anisotropy axes (see the corresponding anisotropic sublattice spin densities in the inset of Fig. 2F).

The energy separation of the spin-up and spin-down states at a given wavevector determined by the electrostatic crystal field is a signature spectroscopy feature of altermagnetism. We see from Fig. 2F, that even if the magnetic exchange field were weaker than the electrostatic crystal field, the latter would still determine the spin separation at momentum states close to the Γ -point. This is a consequence, on one hand, of the weakly wavevector-dependent band splitting by the exchange field (including the Γ -point) and, on the other hand, of the spin-degeneracy of the Γ -point imposed by the spin symmetry of altermagnets. The crystal-field mechanism of the spin-polarization makes the altermagnetic spectroscopy distinct from the established physics of ferromagnetic spin-polarization governed by the spin-exchange field. It also differs fundamentally from the relativistic spin-orbit coupling mechanism.

Figs. 2C-F show the emergence of the spin-polarization when the phase changes from non-magnetic to altermagnetic, i.e., when the molecular exchange field is turned on. A complementary scenario is shown on the antiferromagnetic and altermagnetic models in Fig. 1, where in both cases the molecular exchange field is present, and the spin-polarization is induced by turning on the mutual tilt of the sublattice anisotropies. These two scenarios suggest complementary experimental approaches to design and optimize altermagnetic materials. The first approach starts from crystals with strong and misaligned local anisotropies and then considers the inclusion of magnetic atoms with antiparallel exchange coupling. In the complementary scenario, a crystal anisotropy engineering, e.g. by strain, can be applied to turn antiferromagnetically ordered crystals into altermagnets.

In Fig. 3 we present the symmetry/topology classification and *ab initio* band-structure calculations of insulating CuF_2 with the Néel temperature 69 K [39] and with relatively light elements. Its crystal, shown in Fig. 3A, is a distorted rutile with a monoclinic structure (crystal space group $P2_1/c$) [40]. The altermagnetic spin point group $2^s/m^s (\bar{1} \oplus \bar{1}C_{2z}\mathcal{R}_s)$ implies again a $W = 2$ topology of the spin-momentum interaction. Unlike KRu_4O_8 , however, the mirror transposing symmetry $\mathcal{M}_z\mathcal{R}_s$, which complements the rotation transposing symmetry $C_{2z}\mathcal{R}_s$, generates a bulk-like spin-momentum interaction. This is confirmed by the *ab initio* calculation presented in Fig. 3B. The spin-resolved band structures are plotted in Figs. 3C, D. (We used the DFT+U method with $U = 5$ eV and $J = 1$ eV [40].) Similar to KRu_4O_8 , the spin splitting is in the ~ 100 meV scale in CuF_2 .

Table 1 shows other insulating altermagnetic candidates, including high Néel temperature CoF_3 and FeF_3 [41], with the spin-momentum interaction topological number $W = 4$. Semiconducting MnTe [25] also falls within this topological family. In Fig. 4 we present a detailed discussion of another member of the $W = 4$ family, metallic CrSb with the Néel temperature of 705 K [42]. As shown in Fig. 4A, it crystallizes in the hexagonal NiAs-type structure (crystal space group $P6_3/mmc$) [42, 43]. Its altermagnetic spin point group $6^s/m^s m^s m^s (\bar{3}m \oplus \bar{3}m C_{6z}\mathcal{R}_s)$ contains the mirror transposing symmetry $\mathcal{M}_z\mathcal{R}_s$, which again makes the spin-momentum interaction bulk-like. In addition, it has three transposing mirror planes orthogonal to the three hexagonal crystal axes. This implies a $W = 4$ topology, as confirmed by *ab initio* calculations in Fig. 4B. CrSb has a more complex band structure than in KRu_4O_8 or CuF_2 , as shown in Figs. 4C. Nevertheless, we can still trace a pair of spin-up and spin-down bands (highlighted by grey shading in Fig. 4C) which are spin-degenerate at Γ , L_1 and L_2 points, and spin split by the crystal field when moving away from these high symmetry points. The spin splitting is as high as 1.2 eV, as shown in Fig. 4D. We also note that, unlike KRu_4O_8 , CrSb hosts a remarkable quasiparticle that is four-fold degenerate at the Γ -point and is spin-polarized away from the Γ -point.

Discussion. Although focusing on the fundamentals of altermagnetism, our work prompts further research in several areas of basic and applied condensed matter physics. We begin this outlook section by pointing out that in Fig. 1, the representative structure of the altermagnetic Type-III spin groups corresponds to a parent cuprate of high-temperature superconductivity La_2CuO_4 [44]. While in the altermagnetic panel of Fig. 1, the mutually tilted sublattice anisotropies reflect the realistic crystal structure of La_2CuO_4 , the antiferromagnetic panel of Fig. 1 considers an artificial alignment of the sublattice anisotropies, and by this recovers the spin-unpolarized Type-II spin point group $mmm1^s$ ($mmm \oplus mmm\mathcal{R}_s$). On the other hand, for the realistic mutual tilt of the anisotropies, and assuming a collinear antiparallel magnetic order, La_2CuO_4 falls into the altermagnetic Type-III spin point group $m^s m^s m$ ($2/m \oplus 2/m\mathcal{C}_{2y}\mathcal{R}_s$). The transposing element $\mathcal{C}_{2y}\mathcal{R}_s$ generates a planar $W = 2$ topology of the spin-momentum interaction. Remarkably, the characteristic orbital harmonic of the spin-momentum interaction in altermagnetic La_2CuO_4 is of the d -wave form, which is reminiscent of the d -wave symmetry of the superconducting order parameter in this cuprate. This observation directly points towards a future exploration of the potential coexistence and interplay of altermagnetism and high-temperature superconductivity [45].

Our calculations in KRu_4O_8 , CuF_2 , and CrSb suggest that intriguing but yet unexplored connections might also exist between altermagnetism and topological insulators and semimetals. In this context we note that, on one hand, symmetry prohibits a realization of altermagnetism in one-dimensional chains; they have a \mathcal{PR}_s (and possibly also $t\mathcal{R}_s$) spin symmetry and, therefore, belong to the antiferromagnetic Type-II spin point groups with spin-degenerate bands. On the other hand, we have demonstrated altermagnetic Type-III spin groups in quasi-one-dimensional, quasi-two-dimensional, and three-dimensional insulators and metals. This opens the possibility of searching for topological-insulators and topological-semimetals, including Chern insulators with the quantized Hall effect in high-temperature systems with vanishing internal or external magnetic dipole.

Finally, our symmetry and topology classification, together with *ab initio* calculations in representative crystals, establish altermagnets as a favourable magnetic class for spintronics research and applications. We have shown that altermagnets can have large energy separation of opposite spins in high transition temperature materials composed of abundant light elements. Moreover, they eliminate stray fields and add a protection of spin against magnetic field. Note that the relativistic non-magnetic spin-texture phases share the zero net dipole moment with altermagnets. However, large relativistic spin splitting requires rare heavy elements. In addition, the relativistic phases suffer from spin decoherence even for small-angle elastic scattering off common isotropic impurities. We have illustrated that this obstacle is diminished in altermagnets by the collinearity of spins, and by the sublattice-spin-momentum locking which can generate a large momentum separation in the Brillouin zone of the equal-energy eigenstates with the opposite spin.

Acknowledgements

We acknowledge fruitful interactions with Igor Mazin and Helen Gomonay. This work was supported by the Ministry of Education of the Czech Republic Grants LM2015087, LNSM-LNSpin, LM2018140, Czech Science Foundation Grants No. 19-28375X, and the EU FET Open RIA Grant No. 766566. Funded by the Deutsche Forschungsgemeinschaft (DFG, German Research Foundation) — TRR 288 – 422213477 (project A09 and B05).

-
- [1] L. Néel, *Science* **174**, 985 (1971).
 - [2] L. Landau, E. Lifshitz, *Electrodynamics of Continuous Media Course of Theoretical Physics*, Pergamon, Oxford (1965).
 - [3] L. Šmejkal, Y. Mokrousov, B. Yan, A. H. MacDonald, *Nature Physics* **14**, 242 (2018).
 - [4] N. P. Armitage, E. J. Mele, A. Vishwanath, *Reviews of Modern Physics* **90**, 015001 (2018).
 - [5] Y. Tokura, K. Yasuda, A. Tsukazaki, *Nature Reviews Physics* **1**, 126 (2019).
 - [6] C. J. Bradley, A. P. Cracknell, *The Mathematical Theory of Symmetry in Solids*, Oxford University Press (2010).
 - [7] C. J. Bradley, B. L. Davies, *Reviews of Modern Physics* **40**, 359 (1968).
 - [8] H. Watanabe, H. C. Po, A. Vishwanath, *Science Advances* **4**, eaat8685 (2018).
 - [9] Y. Xu, *et al.*, *Nature* **586**, 702 (2020).
 - [10] W. F. Brinkman, R. J. Elliott, *Proceedings of the Royal Society A: Mathematical, Physical and Engineering Sciences* **294**, 343 (1966).
 - [11] D. B. Litvin, *Acta Crystallographica Section A* **33**, 279 (1977).
 - [12] L. Šmejkal, R. González-Hernández, T. Jungwirth, J. Sinova, *Science Advances* **6**, eaaz8809 (2020).
 - [13] K. Samanta, *et al.*, *Journal of Applied Physics* **127**, 213904 (2020).
 - [14] Z. Feng, *et al.*, arXiv:2002.08712 (2020).
 - [15] H. Reichlova, *et al.*, arXiv:2012.15651 (2020).
 - [16] S. López-Moreno, A. H. Romero, J. Mejía-López, A. Muñoz, I. V. Roshchin, *Physical Review B*

- 85**, 134110 (2012).
- [17] Y. Noda, K. Ohno, S. Nakamura, *Physical Chemistry Chemical Physics* **18**, 13294 (2016).
- [18] K.-H. Ahn, A. Hariki, K.-W. Lee, J. Kuneš, *Physical Review B* **99**, 184432 (2019).
- [19] S. Hayami, Y. Yanagi, H. Kusunose, *Journal of the Physical Society of Japan* **88**, 123702 (2019).
- [20] L.-D. Yuan, Z. Wang, J.-W. Luo, E. I. Rashba, A. Zunger, *Physical Review B* **102**, 014422 (2020).
- [21] S. Hayami, Y. Yanagi, H. Kusunose, *Physical Review B* **102**, 144441 (2020).
- [22] L.-D. Yuan, Z. Wang, J.-W. Luo, A. Zunger, *Physical Review Materials* **5**, 014409 (2021).
- [23] S. A. Egorov, R. A. Evarestov, *The Journal of Physical Chemistry Letters* **12**, 2363 (2021).
- [24] M. Naka, *et al.*, *Nature Communications* **10**, 4305 (2019).
- [25] R. González-Hernández, *et al.*, *Physical Review Letters* **126**, 127701 (2021).
- [26] M. Naka, Y. Motome, H. Seo, *Physical Review B* **103**, 125114 (2021).
- [27] L. Šmejkal, A. B. Hellenes, R. González-Hernández, J. Sinova, T. Jungwirth, arXiv:2103.12664 (2021).
- [28] D.-F. Shao, S.-H. Zhang, M. Li, E. Y. Tsybal, arXiv:2103.09219 (2021).
- [29] D. Gosálbez-Martínez, I. Souza, D. Vanderbilt, *Physical Review B* **92**, 085138 (2015).
- [30] M.-T. Suzuki, T. Koretsune, M. Ochi, R. Arita, *Physical Review B* **95**, 094406 (2017).
- [31] R. A. Evarestov, V. P. Smirnov, *Site Symmetry in Crystals*, vol. 108 of *Springer Series in Solid-State Sciences* (Springer Berlin Heidelberg, Berlin, Heidelberg, 1997).
- [32] R. Winkler, *Spin–Orbit Coupling Effects in Two-Dimensional Electron and Hole Systems*, vol. 191 of *Springer Tracts in Modern Physics* (Springer Berlin Heidelberg, Berlin, Heidelberg, 2003).
- [33] K. Ishizaka, *et al.*, *Nature Materials* **10**, 521 (2011).
- [34] C. Wu, K. Sun, E. Fradkin, S.-C. Zhang, *Physical Review B* **75**, 115103 (2007).
- [35] K. Dewhurst, Elk code.
- [36] W. Kobayashi, *Physical Review B* **79**, 155116 (2009).
- [37] T. Toriyama, M. Watanabe, T. Konishi, Y. Ohta, *Physical Review B* **83**, 195101 (2011).
- [38] D. I. Khomskii, *Transition Metal Compounds* (Cambridge University Press, Cambridge, 2014).
- [39] R. J. Joenk, R. M. Bozorth, *Journal of Applied Physics* **36**, 1167 (1965).
- [40] Y. Zheng, *et al.*, *Solid State Communications* **152**, 1703 (2012).

- [41] S. Lee, *et al.*, *Physica B: Condensed Matter* **551**, 94 (2018).
- [42] I. J. Park, S. Kwon, R. K. Lake, *Physical Review B* **102**, 224426 (2020).
- [43] J. Yuan, Y. Song, X. Xing, J. Chen, *Dalton Transactions* **49**, 17605 (2020).
- [44] C. Lane, *et al.*, *Physical Review B* **98**, 125140 (2018).
- [45] Q. Si, R. Yu, E. Abrahams, *Nature Reviews Materials* **1**, 1 (2016).

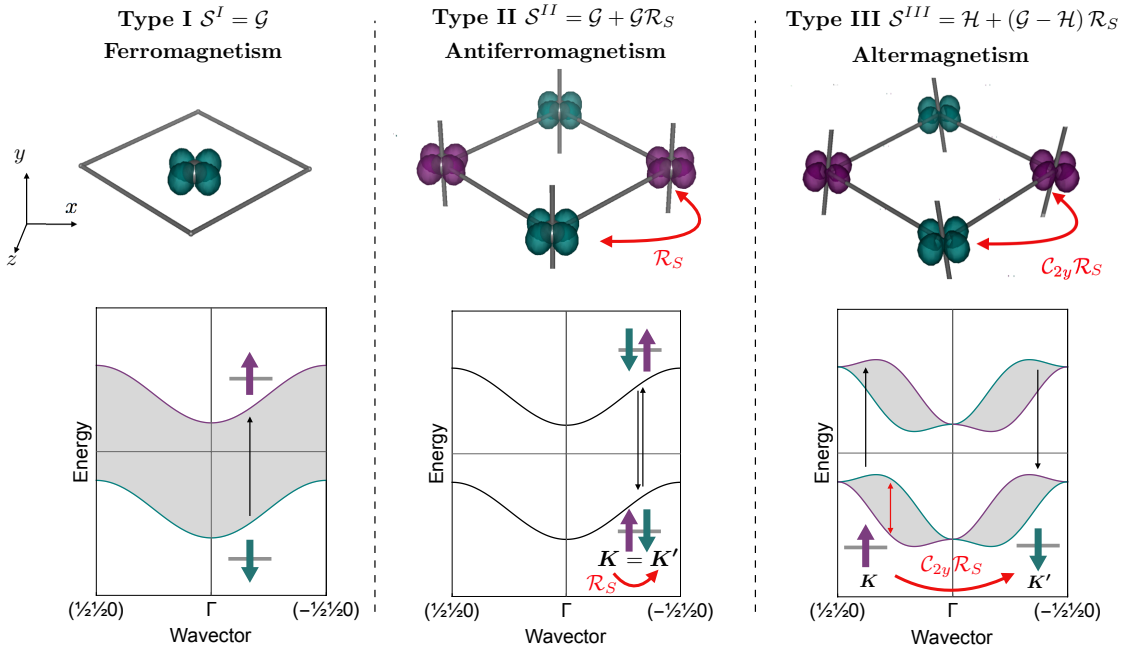


FIG. 1. **Illustration of Type-I ferromagnetic, Type-II antiferromagnetic and Type-III altermagnetic spin point groups.** (Left) Top: A site magnetization density illustrating Type-I ferromagnetic spin point groups without a transposing symmetry element. Bottom: A cartoon of ferromagnetically spin-split bands (green and purple) by the global molecular exchange field (black arrow). (Middle) Top: An illustrative example of magnetization densities on two sublattices (green and purple) with opposite magnetic moments. They correspond to a hypothetical phase of La_2CuO_4 with a Type-II antiferromagnetic spin point group $mmm \oplus mmm\mathcal{R}_s$. Bottom: A cartoon of two spin-degenerate bands, split due to the local molecular exchange field (black arrows). The \mathcal{R}_s -symmetry of the spin point group transforms a state with momentum \mathbf{K} and one spin orientation on an equal-energy state with the same momentum and opposite spin. The two sublattices contribute equally to the state at a given energy and momentum, making the real-space sublattice magnetization invisible in the momentum space. (Right) : Same as (Middle) illustrating magnetization densities in La_2CuO_4 with mutually tilted anisotropy axes, corresponding to a Type-III altermagnetic spin point group $2/m \oplus 2/mC_{2y}\mathcal{R}_s$. In addition to the band-splitting by the local molecular exchange field (black arrows), a spin-splitting of the bands occurs due to the electrostatic crystal field (red double-arrow).

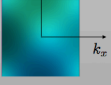
Planar/bulk	Winding number	Point group G	Spin point group S_{III}	Subgroup H	Transposing generator	Characteristic crystal harmonic	Candidate material	
Planar 	$W=2$ 	mmm	$m^S m^S m^S (8)$	$2/m$	C_{2x}	d_{xy}	La_2CuO_4 [42]	
		$4/m$	$4^S/m (8)$	$2/m$	C_{4z}	$d_{x^2-y^2}$	$\text{K}(\text{RuO}_2)_4$ [35]	
		$4/mmm$	$4^S/mmm (16)$	mmm	C_{4z}	d_{xy}	RuO_2 [11,17], MnO_2 [16], MnF_2 [19]	
	$W=4$ 	$4/mmm$	$4/m^S m^S m^S (16)$	$4/m$	C_{2x}	g_{xy}	KMnF_3 [44]	
		$W=6$ 	$6/mmm$	$6/m^S m^S m^S (24)$	$6/m$	C_{21}	i_{xy}	
Bulk 	$W=2$ 	$2/m$	$2^S/m^S (4)$	-1	C_2	d_{zx}	CuF_2 [38]	
		$W=4$ 	$-3m$	$-3m^S (12)$	-3	C_{21}	g_{zxy}	$\text{CoF}_3, \text{FeF}_3$ [39]
	$6/m$		$6^S/m^S (12)$	-3	C_6			
	$6/mmm$		$6^S/m^S m^S m^S (24)$	-3m	C_6	CrSb [41], MnTe [24]		
	$W=6$ 	$m3m$	$m3m^S (48)$	$m3$	C_4	i_{zxy}		

TABLE I. **Topology and spin symmetry groups of altermagnets, and material candidates.** The columns describe, respectively, planar or bulk character (and schematic picture of the corresponding out-of-plane spin-texture in the $k_x - k_z$ plane) of the spin-momentum interaction, spin winding number (and picture of the corresponding in-plane spin-texture in the $k_x - k_y$ plane), crystallographic centrosymmetric point group G , altermagnetic spin point group S_{III} (in the bracket we list number of symmetry elements), halving subgroup H of non-transposing crystal symmetry elements, generator of transposing symmetry elements, characteristic anisotropic crystal harmonic, and altermagnetic candidates with references to respective materials. The crystal harmonics are defined as follows: $d_{xy} = \sin k_x \sin k_y$, $d_{x^2-y^2} = \cos k_x - \cos k_y$, $g_{xy} = d_{xy} d_{x^2-y^2}$, $i_{xy} = d_{xy} (\cos \sqrt{3}k_x - \cos k_y) (\cos \sqrt{3}k_y - \cos k_x)$, $g_{zxy} = d_{zy} (\cos k_x - \cos \sqrt{3}k_y)$, $i_{zxy} = (\cos k_x - \cos k_y) (\cos k_y - \cos k_z) (\cos k_z - \cos k_x)$.

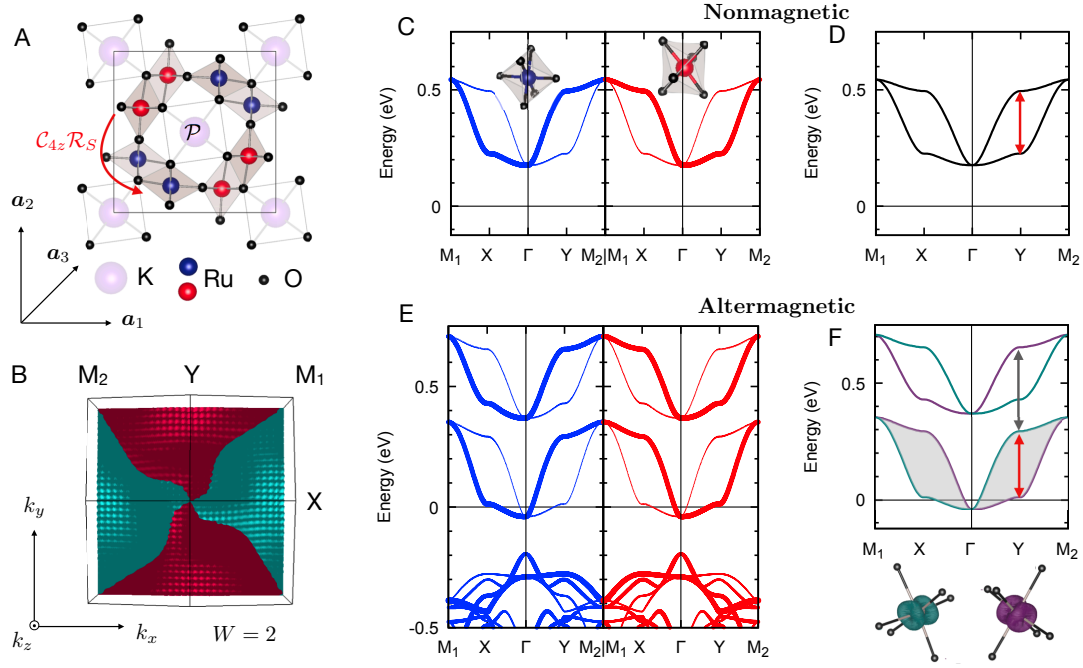


FIG. 2. Symmetry, topology, and spectroscopy in candidate altermagnet KRu_4O_8 . (A) Schematic crystal structure with red and blue Ru sublattices, and with the depicted generator of transposing symmetry elements of the altermagnetic spin point group $2/m \oplus 2/mC_{4z}\mathcal{R}_s$. (B) Calculated spin-momentum interaction with the winding number $W = 2$ on top of the *ab initio* Fermi surface. Purple corresponds to spin-up and green to spin-down. Sublattice (C) and spin (D) projected *ab initio* band structure of the non-magnetic phase. The bands in (D) are split due to the crystal field (red double-arrow), as seen from the comparison to (C), and are spin-degenerate. (E,F) Same as (C,D) for the altermagnetic phase. The insets in (F) show the magnetization densities of the blue and red sublattice with opposite orientation of the magnetic moment (green and purple). The two sublattices lock, respectively, the states with momentum **X** and spin-down (lower green band), and momentum **Y** and spin-up (lower purple band).

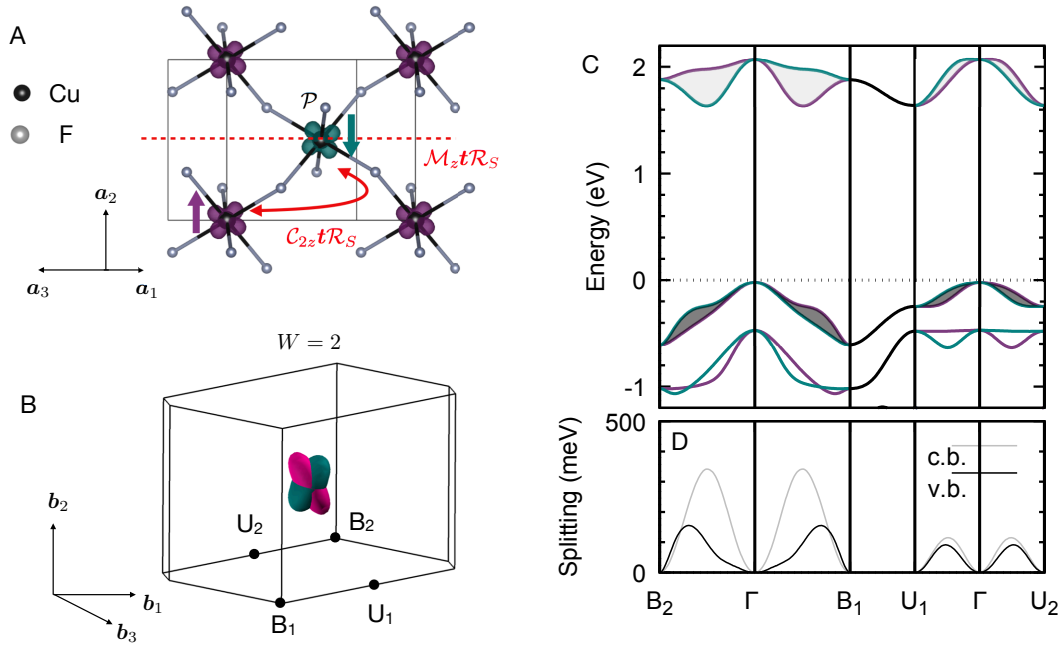


FIG. 3. **Insulating light elements altermagnetic candidate CuF₂.** (A) Schematic crystal structure with Cu sublattices and the respective magnetization densities with opposite orientation of the magnetic moment (purple and green). The altermagnetic spin point group is $\bar{1} \oplus \bar{1}C_{2z}\mathcal{R}_s$. The panel shows transposing symmetries $C_{2z}t\mathcal{R}_s$ and $M_zt\mathcal{R}_s$ ($t = (0, \frac{1}{2}, \frac{1}{2})$). (B) Calculated spin-momentum interaction with the winding number $W = 2$ on top of the *ab initio* Fermi surface for the Fermi level near the top of the valence band. (C) Spin projected *ab initio* band structure in the altermagnetic phase. (D) Wavevector dependence of the spin splitting in the conduction band (grey) and valence band (black).

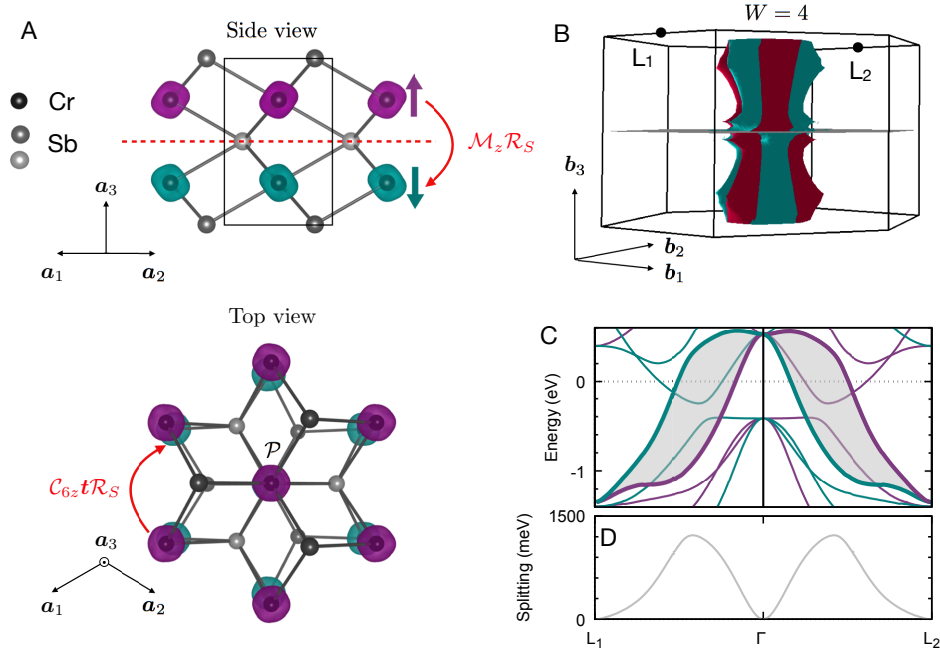


FIG. 4. **Metallic high Néel temperature altermagnetic candidate CrSb.** (A) Schematic crystal structure with Cr sublattices and the respective magnetization densities with opposite orientation of the magnetic moment (purple and green). The altermagnetic spin point group is $\bar{3}m \oplus \bar{3}mC_{6z}\mathcal{R}_s$. The panel shows transposing symmetries $C_{6z}t\mathcal{R}_s$ and $M_z\mathcal{R}_s$ ($t = (0, 0, \frac{1}{2})$). (B) Calculated spin-momentum interaction with the winding number $W = 4$ on top of the *ab initio* Fermi surface. (C) Spin projected *ab initio* band structure in the altermagnetic phase. (D) Wavevector dependence of the spin splitting between the bands highlighted in (C) by the grey shading.